Modeling electrical currents through an ion-selective membrane in the overlimiting regime

By X. I. A. Yang†, K. M. Wang, H. H. A. Xu† AND A. Mani

When a sufficiently high voltage is applied, ion transport between an aqueous electrolyte and an ion-selective membrane is dominated by chaotic convection of cations and anions. One notable feature of electroconvection is the highly unsteady vortices owing to nonlinear interactions between charge transport and fluid motions that span a wide range of scales. In this work, we model the current density at the membrane surface using the canonical multifractal formalism. From this, we obtain definite predictions for the scaling behavior of moments of temporally filtered electrical currents, a scaling transition in the two-point correlation, and electrical current power spectra with a slope shallower than -1, which are validated by comparison with direct numerical simulation data of chaotic electroconvection in a two-dimensional plane channel. This illustrates how one might successfully model the statistics of electric current fluctuations between an electrolyte and an ion-selective membrane by analogy with a self-similar cascade process from large to small scales.

1. Introduction

Ion-selective materials are widely used in electrodialysis systems (Mani 1991; Scott 1995; Vera *et al.* 2007; Cheng & Guo 2009; Weber *et al.* 2011). A basic membrane-electrolyte system contains an ion-selective membrane, an aqueous electrolyte, and an electrical potential difference between the ion reservoir and the membrane (Schoch *et al.* 2008; Nikonenko *et al.* 2010). The model system is sketched in Figure 1(a). An electrical current occurs as a result of the applied electric potential difference, i.e., the applied voltage. Figure 1(b) shows a sketch of the current as a function of the applied voltage. The electrical current increases linearly as a function of the applied voltage for sufficiently low voltages (Levich & Tobias 1963). It reaches a limiting current, beyond which an increase in the voltage no longer leads to an increase in the current. However, above a critical voltage, the overlimiting current regime appears (Kim *et al.* 2007; Yossifon & Chang 2008; Kim *et al.* 2012; Kwak *et al.* 2013). In this work, we study the behavior of the electrical current in the overlimiting regime. In this regime, a mixing layer emerges between the ion reservoir and the ion-selective membrane. Ion transport in the mixing layer becomes chaotic owing to the now well-known electroconvective instability (Rubinstein & Zaltzman 2000).

The transport of cations, anions, and fluid in the model system is governed by the following coupled Stokes-Poisson-Nernst-Planck equations

$$0 = -\nabla p + \mu\nabla^2\mathbf{v} - ze(c^+ - c^-)\nabla\phi, \tag{1.1}$$

$$\nabla\cdot\mathbf{v} = 0, \tag{1.2}$$

† Department of Mechanical and Nuclear Engineering, Pennsylvania State University

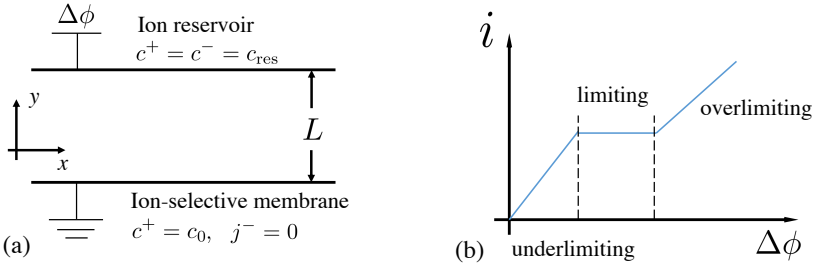

FIGURE 1. (a) Schematics of the model system. The system contains (i) a stationary ion reservoir at the top boundary, where both the cation and the anion concentrations are constant; (ii) an ion-selective membrane at the bottom boundary, where the cation concentration is constant and the anion flux is zero; and (iii) an electrical potential difference $\Delta\phi$ between the reservoir and the membrane. The ion reservoir is at a distance L from the ion-selective membrane. (b) Electrical current as a function of the applied voltage. The current exhibits an ohmic behavior in the underlimiting regime. The current plateaus in the limiting regime owing to concentration polarization (Probstein 2005). At a critical voltage, the system enters the overlimiting regime, where V_T is the thermal voltage.

$$\frac{\partial c^{\pm}}{\partial t} = -\nabla \cdot \left(c^{\pm}\mathbf{v} - D\nabla c^{\pm} \mp D\frac{ze}{k_B T} c^{\pm}\nabla\phi \right), \tag{1.3}$$

$$-\varepsilon\nabla^2\phi = ze(c^+ - c^-). \tag{1.4}$$

Here, Eq. (1.1) is the Stokes equation with an incorporated electric body force, t is time, $\mathbf{v}$ is the velocity vector, p is the deviation from the static pressure, μ is the dynamic viscosity, e is the elementary charge, $z = z^+ = z^-$ is the ionic valence, c^+ and c^- are the cationic and anionic concentration, respectively, and ϕ is the electrostatic potential. The physical size of typical membrane-electrolyte channels in electrochemical devices is usually very small. These devices usually operate at quite small Reynolds numbers. Hence, we neglect the inertia force (the material derivative) and retain only the momentum balance between pressure, viscous, and electrostatic forces in Eq. (1.1). Equation (1.2) is the fluid continuity equation. Equation (1.3) is the ion transport equation using Nernst-Planck fluxes, $D = D^+ = D^-$ is the electrolyte diffusivity, k_B is the Boltzmann constant, and T is the reference temperature. Last, Eq. (1.4) is the electrostatic Poisson equation, and ε is the electrical permittivity. Different from hydrodynamic instabilities, which are usually a result of fluid inertia, the electroconvective instability is owing to the coupling between the Stokes equation and the Nernst-Planck equation through the electric potential term, $\nabla\phi$ (see, e.g., (Rubinstein *et al.* 2008)). In addition to the dimensions of the model system (the aspect ratio of the channel), the ion transport between the reservoir and the membrane is governed by the nondimensional numbers, including the electrohydrodynamic coupling constant κ and the electric double layer thickness ϵ

$$\kappa = \frac{\varepsilon}{\mu D}\left(\frac{k_B T}{ze}\right)^2, \quad \epsilon = \frac{1}{L}\sqrt{\frac{\varepsilon k_B T}{2(ze)^2 c_{\text{res}}}}, \tag{1.5}$$

where c_{res} is the ion concentration at the reservoir. Typical values of the two nondimensional numbers are $\kappa \sim O(1)$, $\epsilon \sim O(10^{-4} - 10^{-6})$ (Druzgalski *et al.* 2013; Druzgalski & Mani 2016). Unless otherwise noted, we use the following quantities for normalization purposes

$$l_0 = L, \quad t_0 = \frac{L^2}{D}, \quad v_0 = \frac{D}{L}, \quad V_T = \frac{k_B T}{ze}, \quad j_0 = \frac{D c_{\text{res}}}{L}, \tag{1.6}$$

where t_0 is the diffusion timescale, v_0 is the diffusion velocity scale, V_T is the thermal voltage, and j_0 is the diffusion electrical current.

The electrical current density is measured by $\mathbf{i} = \mathbf{j}^+ - \mathbf{j}^-$, where $\mathbf{j}^\pm = c^\pm \mathbf{v} - \nabla c^\pm \mp c^\pm \nabla\phi$. Although limited to $\epsilon \sim O(10^{-3} - 10^{-4})$ owing to the high computational cost needed to simulate smaller ϵ (Karatay *et al.* 2015), direct numerical simulations (DNS) have been useful for probing the details of electroconvection. DNS directly solves the governing equations, i.e., Eqs. (1.1) to (1.4), and all ion transport information is readily available from the DNS solutions. Here, we briefly review a few previous works. Overlimiting current had long been observed experimentally, but its cause was debated (Nikonenko *et al.* 2014). Although a number of mechanisms were proposed, it wasn't until recently that a plausible description emerged from the stability analysis of an idealized system by Rubinstein & Zaltzman (2000) and the following works by Zaltzman & Rubinstein (2007) and Abu-Rjal *et al.* (2016). Since then, experiments confirmed the presence of electroconvective vortices (de Valença *et al.* 2015) and a number of studies utilizing 2D and 3D DNS were performed (Pham *et al.* 2012; Druzgalski *et al.* 2013; Demekhin *et al.* 2013, 2014; Druzgalski & Mani 2016). Druzgalski *et al.* (2013) and Druzgalski & Mani (2016) showed the multiscale structure of chaotic electroconvection and reported power spectra of the fluid kinetic energy and ion concentrations. Other DNS studies emerged studying electroconvection on curved surfaces (Chang *et al.* 2012), confinement (Andersen *et al.* 2017), patterning (Davidson *et al.* 2016), and buoyancy (Karatay *et al.* 2016). In this work, we use the canonical setting and model the current density at the ion-selective membrane. In particular, we study the formation of current anomaly and advection of the anomalies.

Figure 2 shows sample current density signals on ion-selective membranes in three DNS of the model system at three voltages, i.e., $\Delta\phi = 60$, $\Delta\phi = 120$, and $\Delta\phi = 240$. The DNS are two-dimensional. The periodic extent is $L_x = 6$. The signals are increasingly more intermittent as a function of the applied voltage. Here, a signal is intermittent if it suffers extreme deviations from its mean. A similar observation was previously made for signals of turbulent dissipation rates in hydrodynamic turbulence, where the energy transfers from large-scale motions to small scales like a cascade. The dissipation rate in isotropic turbulence is increasingly more intermittent as the Reynolds number increases (Meneveau & Sreenivasan 1991). The similar intermittent fluctuations of current density on the ion-selective membrane in the overlimiting regime and the dissipation rate in hydrodynamic turbulence suggest that it might be possible to apply similar modeling tools to fit and predict new scalings of the statistics of the current density. Here, we apply the multifractal framework to test this hypothesis.

The rest of the paper is organized as follows. In Section 2, we propose a physics-based model for current density on ion-selective membranes. In Section 3, we compare the model to DNS data. Concluding remarks are given in Section 4.

2. A multifractal model for current density on ion-selective membranes

We model the electrical current transport from the reservoir to the membrane as a cascade, where the current j cascades from large scales to small scales, and from small scales to even smaller ones, which continues to the electric screening scale ($\sim \epsilon$). Figure 3 shows a schematic of the modeled electrical current transport. The analysis focuses on electrical current signals in the temporal domain. The cascade process may be thought of as one of large scales breaking into small scales while passing their electrical currents

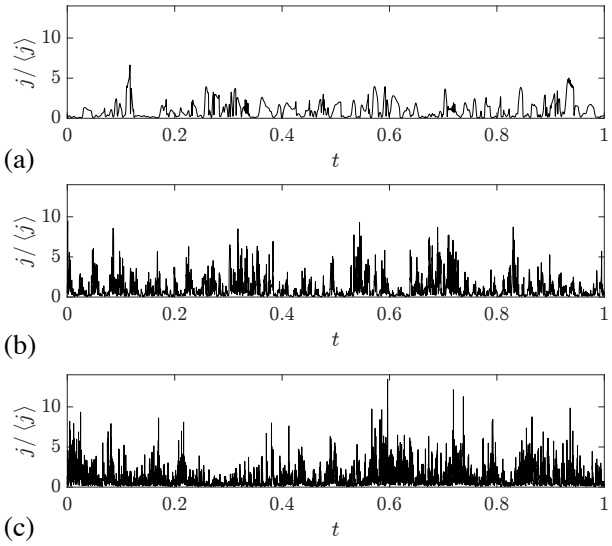

FIGURE 2. Sample current density signals normal to an arbitrarily chosen location on the ion-selective membrane for (a) $\Delta\phi = 60$, (b) $\Delta\phi = 120$, and (c) $\Delta\phi = 240$. The signals are normalized by their respective means. $\langle\cdot\rangle$ is the time average of the bracketed quantity.

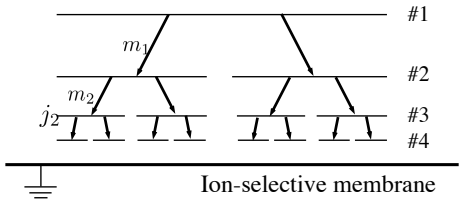

FIGURE 3. Schematic of the modeled current transport process. Without loss of generality, a binary partition of the current from the large scale to the neighboring small scale is sketched (Frisch 1995). It is worth noting the developed model is temporal only.

to the small scales. We may model this cascade process using a random multiplicative model (Frisch 1995),

$$\frac{\tilde{j}_{\delta t}}{\langle j_w\rangle} = \prod_{i=1}^{N_{\delta t}} m_i, \quad N_{\delta t} \sim \log(T/\delta t), \tag{2.1}$$

where $\tilde{j}_{\delta t}$ is the temporally filtered instantaneous electrical current at a filtration timescale δt, $\langle j_w\rangle$ is the time-averaged electrical current at the ion-selective membrane, and m_is are identically, independently distributed random multipliers (or factors) that represent the electrical current from a large scale $\delta t \sim T/2^i$ to a small scale $\delta t \sim T/2^{i+1}$, where T is some integral timescale. To conserve the mean electrical current, we constrain the multipliers such that their mean is 1. It follows that the number of multipliers is $N_{\delta t} \sim \log(T/\delta t)$. In Figure 3, we sketched the current at scale #3. Scale #1 passes $m_1/1$ (may involve a local current density) of its current to scale #2, which then passes $m_2/1$ of its current to scale #3. The current $\tilde{j}_2$ is therefore $\tilde{j}_2/\langle j_w\rangle = m_1 \times m_2$. The same random multiplicative process was used to model the energy cascade process in hydrodynamic turbulence (Meneveau & Sreenivasan 1987; She & Leveque 1994). It is worth noting that although a cascade process may be modeled by a multifractal model, a

process that can be modeled by a multifractal model is not necessarily a cascade process, although there is little discussion on the alternatives to a cascade process (Spalart 2017, private communication). With that added caveat in mind, we note that if the DNS data compare well with the model, we can validate only the random multiplicative model, i.e., Eq. (2.1), but not the electrical current cascade.

Next, we briefly discuss the scaling implications of Eq. (2.1). First, we compute the moments of the temporally filtered electrical current.

$$\langle \tilde{j}_{\delta t}^{q} \rangle \sim \left\langle \prod_{i=1}^{N_{\delta t}} m_i^q \right\rangle = \prod_{i=1}^{N_{\delta t}} \langle m_i^q \rangle = \exp(N_{\delta t})^{\log(\langle m^q \rangle)} \sim \left(\frac{T}{\delta t} \right)^{\tau(q)}, \quad \tau(q) = \log\left(\langle m^q \rangle\right), \tag{2.2}$$

leading to power-law scalings of the central moments as a function of the filtration timescale δt. Here, m is a random multiplicative that has the same statistical properties as m_i in Eq. (2.1). We have also used the identity $a^{\log(b)} = b^{\log(a)}$, where a, b are positive real numbers, and invoked the modeling assumption that the m_i are independently distributed random multipliers. Because time filtration is linear, using a straightforward top-hat filtering in the Fourier space $\langle \tilde{j}_{\delta t} \rangle$ is trivially equal to the time-mean wall current $\langle j_w \rangle$. This poses one constraint on the power-law exponent, i.e., $\tau(q = 1) = 0$. In addition, by definition, $\langle \tilde{j}_{\delta t}^{0} \rangle = 1$, which leads to a second constraint, i.e., $\tau(q = 0) = 0$. If the random multipliers are Gaussian, i.e., if the multipliers in Eq. (2.1) are Gaussian variables, it follows from Eq. (2.2) that the power-law exponent is a quadratic function of q, i.e., $\tau_g(q) \sim q^2$ Bulmer (1979). Taking into account the abovementioned two constraints, we get $\tau_g(q) = C_1 \left[(q - 1/2)^2 - 1/4 \right]$, where the subscript g indicates Gaussian approximation.

The power-law exponent $\tau(q)$ is the counterpart of the anomalous exponent in hydrodynamic turbulence, where the anomalous exponent is the exponent $\zeta(q)$ in $\langle \Delta u^q \rangle \sim l^{\zeta}(q)$ with Δu being the velocity difference between two points that are displaced by a distance l. If the electrical current is divided equally between scales, the resulting electrical current will be nonintermittent and space filling (time filling), and the power-law exponent will be $\tau(q) \equiv 0$. The fact that $\tau(q)$ is not constant but a function of q shows that the electrical current is not space filling/time filling (Meneveau *et al.* 1990). The predicted power-law scaling can only be found within a range of temporal scales where the multipliers are approximately self-similar. Their range depends on the scale cutoffs sketched in Figure 3. The large-scale cutoff is approximately the distance between the reservoir and the membrane, and the small-scale cutoff is approximately the electric screening length. The scale cutoffs in the time domain are proportional to those in the spatial domain. DNS is known to be costly for multiscale problems (Choi & Moin 2012), and the existing data of the model system in Figure 1 contain only a moderate range of scales between the large- and small-scale cutoffs, within which the multiplier is identically distributed. Consequently, the power-law scaling in Eq. (2.2) may only be found across a limited range of scales, beyond which the motions and the corresponding multipliers are affected by the electric screening or the large scales and therefore are not self-similar. To reinstate self-similarity, a useful trick is the so-called extended self-similarity, where one plots the scaling of $\langle \tilde{j}_{\delta t}^{q} \rangle$ as a function of $\langle \tilde{j}_{\delta t}^{q_o} \rangle$—the former is a power-law function of the latter as long as the multipliers are statistically independent (Yang *et al.* 2016*b*) (thus relaxing the self-similarity assumption).

Second, we compute the two-time correlation $\langle j_w^{q_1}(t) j_w^{q_2}(t + \delta t) \rangle$, where j_w is the instantaneous electrical current at the membrane, δt is the time delay, and q_1, q_2 are two real numbers. Following the previous works (O'Neil & Meneveau 1993; Yang *et al.* 2016*a*),

if a signal can be modeled by a random multiplicative process, the two-time correlation satisfies

$$\langle j_w^{q_1}(t) j_w^{q_2}(t+\delta t)\rangle \sim (\delta t/T)^{\Phi(q_1,q_2)}, \quad \Phi(q_1,q_2) = \min\left[\tau(q_1)+\tau(q_2)-\tau(q_1+q_2), 1\right], \tag{2.3}$$

which can be interpreted as a power-law scaling and a scaling transition at $\tau(q_1)+\tau(q_2)-\tau(q_1+q_2)=1$. If the m_is are Gaussian, i.e., if $\tau(q) = C_1[(q-1/2)^2 - 1/4]$, the power-law exponent $\Phi(q_1,q_2)$ in Eq. (2.3) will be $\Phi_g(q_1,q_2) = -2C_1 q_1 q_2$. The scaling transition is conventionally considered conclusive evidence of a tree-like hierarchical process (Biferale 2003); therefore verifying the scaling transition will be at the center of the present work.

Last, we compute the power spectrum of the electrical current. The power spectrum is but the Fourier transform of $\langle j_w(t) j_w(t+\delta t)\rangle$, which according to Eq. (2.3) is $\langle j_w(t) j_w(t+\delta t)\rangle \sim (\delta t/T)^{-\tau(2)}$. It follows that the power spectra are

$$E_{jj} \sim f^{-1+\tau(2)}, \tag{2.4}$$

leading to a slightly shallower slope than -1. Here, we have invoked $\tau(1) = 0$.

3. Comparing the model to DNS data

We compare the model to DNS. The DNS directly solves Eqs. (1.1) to (1.4) with the top wall boundary conditions $\mathbf{v} = 0$, $\phi = \Delta\phi$, $c^+ = c^- = 1$ and the bottom wall boundary conditions $\mathbf{v} = 0$, $\phi = 0$, $j_y^- = 0$, $c^+ = c_0^+$. We vary the electric potential difference $\Delta\phi$ from 60 to 240. The electric forcing increases as the electric potential difference, leading to larger concentration gradients. The analysis here focuses on the $\Delta\phi = 120$ case, for which, the data are mostly converged. A grid of size 960×180 (grid points) is used for that case. A second-order finite difference is used for spatial discretization. The grid is stretched in the wall-normal direction away from the ion-selective membrane. A second-order scheme is used for time marching. Details of the code may be found in Karatay *et al.* (2015) and the references cited therein. The statistics are time averaged over 10 diffusion timescales.

Figure 4(a) shows the central moments of the time-filtered electrical current as functions of the filtration time. The electrical current at the wall is positive definite; therefore raising $\tilde{j}_{\delta t}$ to $q < 0$ power is not problematic. The power-laws in Eq. (2.2) are found within $0.003 < \delta t < 0.01$. Although only a limited range of timescales are fit well by this power-law scaling, we expect a more extended scaling range to occur for higher voltages or if one adopts the extended self-similarity scaling. Figure 4(b) shows the extended self-similarity scalings, and the extents of the power-law scalings are wider than those in Figure 4(a). The measured power-law exponent is shown as a function of q in Figure 4(c), along with the Gaussian approximation. The constant C in $\tau_g(q)$ is obtained by fitting the data near $q = 0$. The data are sub-Gaussian, so that j_w is less intermittent than a Gaussian random process (Yang & Lozano-Durán 2017).

Next, we look at the two-point statistics. Following previous works on scaling transition in the context of hydrodynamic turbulence (O'Neil & Meneveau 1993; Yang *et al.* 2016*a*), we focus on the case $q_1 = -q_2$. Figure 5(a) shows $\langle j_w^q(t) j_w^{-q}(t+\delta t)\rangle$ as functions of the two-point time delay for q from 0.5 to 3.5. A power-law scaling is found in $0.001 < \delta t < 0.003$. The measured power-law exponent $\Phi(q,-q)$ is shown as a function of q in Figure 5(b), and the predicted scaling transition is indeed found. This finding lends strong support to the model in Section 2 and shows evidence for the tree-like hierarchical structure in Figure 3(a).

Finally, Figure 6 shows the computed power spectra of the electrical current at the three

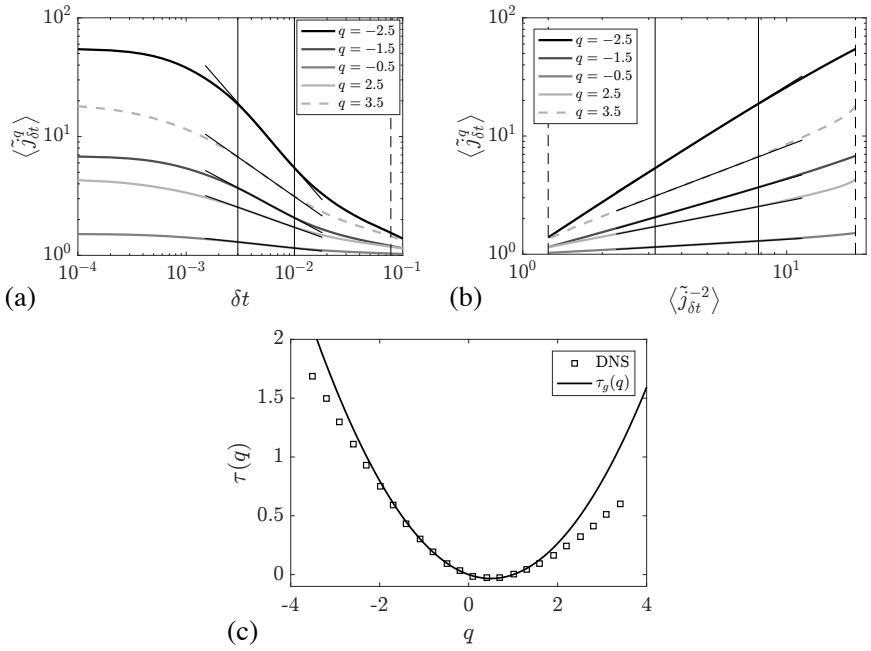

FIGURE 4. (a) Central moments of the time-filtered electrical current (a straightforward top-hat filter in Fourier space is used). We have enclosed the range where a power-law scaling is found. (b) Extended self-similarity scalings. The enclosed regions correspond to those in panel (a). (c) Power-law exponent. The Gaussian model corresponds to $\tau_g(q) = 0.13\left[(q-1/2)^2 - 1/4\right]$.

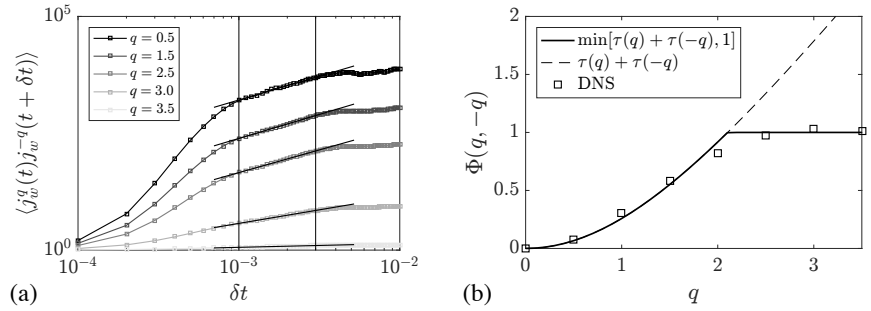

FIGURE 5. (a) $\left\langle j^q_w(t) j^{-q}_w(t+\delta t) \right\rangle$ as functions of δt for $q = 0.5$, 1.5, 2.5, 3.0, 3.5. (b) Measured power-law exponent $\Phi(q, -q)$. $\tau(q)$ is the measured exponent of $\langle \tilde{j}^q_{\delta t} \rangle$.

electrical potentials. Although Eq. (2.4) is not a good approximation of the simulation data at low voltages, at higher applied voltages $\Delta\phi = 240$, the power spectrum follows the model prediction across a wider range of scales (over a decade in frequency), again lending support to our multiplicative cascade model described in Section 2.

4. Conclusions

Electroconvection near an ion-selective material has applications in many industries for its ability to enhance ion transport. Research into electroconvection has recently progressed rapidly with the availability of new measurement techniques and computational

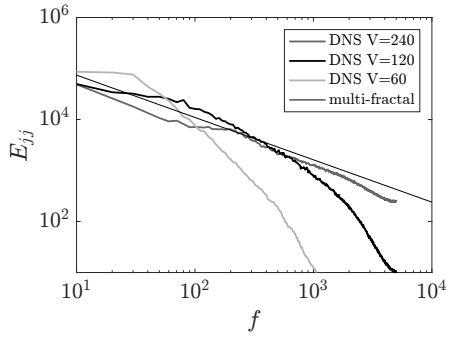

FIGURE 6. Power spectra of the electrical current at the membrane for $\Delta\phi = 60$, 120, 240. The multifractal model prediction, i.e., Eq. (2.4), is shown with a thin solid line, and the slope is $-1 + \tau(2) = -0.83$.

resources. High-fidelity simulation aids the development of cheap-to-evaluate reduced-order models. In this work, we provided some evidence showing that the electrical current at the wall may be modeled as a random multiplicative process, where the electrical current is passed down from large scales to small scales through a cascade process. However, this model is but the first step toward understanding the physics behind the coupled governing equations.

Acknowledgments

XY thanks the CTR Summer Program for financial support. XY acknowledges P. Moin, J. Jimenez, B. Farrell, S.-S. He, P. Johnson and M. Howland for fruitful discussions, and M.P. Encinar and C. Hamman for reviewing the preliminary version of the manuscript.

REFERENCES

ABU-RJAL, R., RUBINSTEIN, I. & ZALTZMAN, B. 2016 Driving factors of electroconvective instability in concentration polarization *Phys. Rev. Fluids* **1**, 1-17.

ANDERSEN, M. B., VAN SOESTBERGEN, M., MANI, A., BRUUS, H., BIESHEUVEL, P. & BAZANT, M. 2012 Current-induced membrane discharge. *Phys. Rev. Lett.* **109**, 108301.

ANDERSEN, M. B., WANG, K. M., SCHIFFBAUER, J. & MANI, A. 2017 Confinement effects on electroconvective instability. *Electrophoresis* **38**, 702–711.

BIFERALE, L. 2003 Shell models of energy cascade in turbulence. *Annu. Rev. Fluid Mech.* **35**, 441–468.

BULMER 1979 *Principles of statistics*. Dover Publications.

CHANG, H.-C., DEMEKHIN, E. A. & SHELISTOV, V. S. 2012 Competition between Dukhin's and Rubinstein's electrokinetic modes. *Phy. Rev. E* **86**, 046319.

CHENG, L.-J. & GUO, L. J. 2009 Ionic current rectification, breakdown, and switching in heterogeneous oxide nanofluidic devices. *ACS Nano* **3**, 575–584.

CHOI, H. & MOIN, P. 2012 Grid-point requirements for large eddy simulation: Chapman's estimates revisited. *Phys. Fluids* **24**, 011702.

DAVIDSON, S. M., ANDERSEN, M. B. & MANI, A. 2014 Chaotic induced-charge electro-osmosis. *Phys. Rev. Lett.* **112**, 128302.

Davidson, S. M., Wessling, M. & Mani, A. 2016 On the dynamical regimes of pattern-accelerated electroconvection. *Sci. Rep.* **6**, 22505.

Demekhin, E., Nikitin, N. & Shelistov, V. 2013 Direct numerical simulation of electrokinetic instability. *Phys. Fluids* **25**, 122001.

Demekhin, E., Nikitin, N. & Shelistov, V. 2013 Three-dimensional coherent structures of electrokinetic instability. *Phys. Rev. E* **90**, 013031.

Druzgalski, C., Andersen, M. & Mani, A. 2013 Direct numerical simulation of electroconvective instability and hydrodynamic chaos near an ion-selective surface. *Phys. Fluids* **25**, 110804.

Druzgalski, C. & Mani, A. 2016 Statistical analysis of electroconvection near an ion-selective membrane in the highly chaotic regime. *Phys. Rev. Fluids* **1**, 073601.

Dydek, E. V., Zaltzman, B., Rubinstein, I., Deng, D., Mani, A. & Bazant, M. Z. 2011 Overlimiting current in a microchannel. *Phys. Rev. Lett.* **107**, 118301.

Femmer, R., Mani, A. & Wessling, M. 2015 Ion transport through electrolyte/polyelectrolyte multi-layers. *Sci. Rep.* **5**, 11583.

Frisch, U. 1995 *Turbulence: The Legacy of AN Kolmogorov*. Cambridge University Press.

Karatay, E., Andersen, M. B., Wessling, M. & Mani, A. 2016 Coupling between buoyancy forces and electroconvective instability near ion-selective surfaces. *Phys. Rev. Lett.* **116**(19), 194501.

Karatay, E., Druzgalski, C. L. & Mani, A. 2015 Simulation of chaotic electrokinetic transport: performance of commercial software versus custom-built direct numerical simulation codes. *J. Colloid Interf. Sci.* **446**, 67–76.

Khair, A. S. 2011 Concentration polarization and second-kind electrokinetic instability at an ion-selective surface admitting normal flow. *Phys. Fluids* **23**, 072003.

Kim, S. J., Ko, S. H., Kwak, R., Posner, J. D., Kang, K. H. & Han, J. 2012 Multi-vortical flow inducing electrokinetic instability in ion concentration polarization layer. *Nanoscale* **4**, 7406–7410.

Kim, S. J., Wang, Y.-C., Lee, J. H., Jang, H. & Han, J. 2007 Concentration polarization and nonlinear electrokinetic flow near a nanofluidic channel. *Phys. Rev. Lett.* **99**, 044501.

Kwak, R., Guan, G., Peng, W. K. & Han, J. 2013 Microscale electrodialysis: concentration profiling and vortex visualization. *Desalination* **308**, 138–146.

Levich, V. G. & Tobias, C. W. 1963 Physicochemical hydrodynamics.*J. Electrochem. Soc.* **110** 251C-252C

Mani, K. 1991 Electrodialysis water splitting technology. *J. Membrane Sci.* **58**, 117–138.

Meneveau, C. & Sreenivasan, K. 1987 Simple multifractal cascade model for fully developed turbulence. *Phys. Rev. Lett.* **59**, 1424.

Meneveau, C. & Sreenivasan, K. 1991 The multifractal nature of turbulent energy dissipation. *J. Fluid Mech.* **224**, 429–484.

Meneveau, C., Sreenivasan, K., Kailasnath, P. & Fan, M. 1990 Joint multifractal measures: theory and applications to turbulence. *Phys. Rev. A* **41** (2), 894.

Nikonenko, V. V., Kovalenko, A. V., Urtenov, M. K., Pismenskaya, N., Han, J., Sistat, P. & Pourcelly, G. 2014 Desalination at overlimiting currents: state-of-the-art and perspectives. *Desalination* **342** 85-106.

Nikonenko, V. V., Pismenskaya, N. D., Belova, E. I., Sistat, P., Huguet, P., Pourcelly, G. & Larchet, C. 2010 Intensive current transfer in membrane

systems: modelling, mechanisms and application in electrodialysis. *Adv. Colloid Interfac.* **160**, 101–123.

O'Neil, J. & Meneveau, C. 1993 Spatial correlations in turbulence: predictions from the multifractal formalism and comparison with experiments. *Phys. Fluids* **5**, 158–172.

Pham, V. S., Li, Z., Lim, K. M., White, J. K. & Han, J. 2012 Direct numerical simulation of electroconvective instability and hysteretic current-voltage response of a permselective membrane. *Phys. Rev. E* **86**, 046310.

Probstein, R. F. 2005 *Physicochemical Hydrodynamics: An Introduction*. John Wiley & Sons.

Rösler, H.-W., Maletzki, F. & Staude, E. 1992 Ion transfer across electrodialysis membranes in the overlimiting current range: chronopotentiometric studies. *J. Membrane Sci.* **72**, 171–179.

Rubinstein, I. & Zaltzman, B. 2000 Electro-osmotically induced convection at a permselective membrane. *Phys. Rev.* **62**, 2238-2251.

Rubinstein, S. M., Manukyan, G., Staicu, A., Rubinstein, I., Zaltzman, B., Lammertink, R. G., Mugele, F. & Wessling, M. 2008 Direct observation of a nonequilibrium electro-osmotic instability. *Phy. Rev. Lett.* **101**, 236101.

Schoch, R. B., Han, J. & Renaud, P. 2008 Transport phenomena in nanofluidics. *Rev. Mod. Phys.* **80**, 839.

Scott, K. 1995 *Handbook of Industrial Membranes*. Elsevier.

She, Z.-S. & Leveque, E. 1994 Universal scaling laws in fully developed turbulence. *Phys. Rev. Lett.* **72**, 336.

Simons, R. 1979 Strong electric field effects on proton transfer between membrane-bound amines and water. *Nature* **280**, 824.

de Valença, J. C., Wagterveld, R. M., Lammertink, R. G. & Tsai, P. A. 2015 Dynamics of microvortices induced by ion concentration polarization. *Phy. Rev. E* **92**, 031003.

Vera, E., Sandeaux, J., Persin, F., Pourcelly, G., Dornier, M. & Ruales, J. 2007 Deacidification of clarified tropical fruit juices by electrodialysis. Part I. Influence of operating conditions on the process performances. *J. Food Eng.* **78**, 1427–1438.

Weber, A. Z., Mench, M. M., Meyers, J. P., Ross, P. N., Gostick, J. T. & Liu, Q. 2011 Redox flow batteries: a review. *J. Appl. Electrochem.* **41**, 1137.

Yang, X. I. A. & Lozano-Durán, A. 2017 A multifractal model for the momentum transfer process in wall-bounded flows. *J. Fluid Mech.* **824**, R2.

Yang, X. I. A., Marusic, I. & Meneveau, C. 2016*a* Moment generating functions and scaling laws in the inertial layer of turbulent wall-bounded flows. *J. Fluid Mech.* **791**.

Yang, X. I. A., Meneveau, C., Marusic, I. & Biferale, L. 2016*b* Extended self-similarity in moment-generating-functions in wall-bounded turbulence at high Reynolds number. *Phys. Rev. Fluids* **1**, 044405.

Yossifon, G. & Chang, H.-C. 2008 Selection of nonequilibrium overlimiting currents: universal depletion layer formation dynamics and vortex instability. *Phys. Rev. Lett.* **101**, 254501.

Zaltzman, B. & Rubinstein, I. 2007 Electro-osmotic slip and electroconvective instability. *J. Fluid Mech.* **579**, 173-226.